Research Square

Preprints are preliminary reports that have not undergone peer review.
They should not be considered conclusive, used to inform clinical practice,
or referenced by the media as validated information.

Artificial Intelligence–Driven Volumetric Quantification of Urinary Stone Burden and Hydronephrosis From CT Images

Hsiang-Ying Lee
Kaohsiung Medical University Hospital, Kaohsiung Medical University
Chun-Kai Chang
Kaohsiung Medical University Hospital, Kaohsiung Medical University
Wei-Ming Li
Kaohsiung Medical University Hospital, Kaohsiung Medical University
Yow-Ling Shiue
National Sun Yat-sen University
Cheng-Tang Pan
National Sun Yat-sen University
Wen-Jeng Wu
Kaohsiung Medical University Hospital, Kaohsiung Medical University
Vineet Gauhar
Ng Teng Fong General Hospital
Karl Marvin Tan
Veterans Memorial Medical Center
Jomari Jalipa
Veterans Memorial Medical Center
Ming-Chan Lee
mclee@mem.nsysu.edu.tw

National Sun Yat-sen University

Research Article

Keywords: urolithiasis, kidney calculi, hydronephrosis, artificial intelligence, deep learning, tomography, x-ray computed

Posted Date: November 3rd, 2026

DOI: https://doi.org/10.21203/rs.3.rs-11359792/v1

License: This work is licensed under a Creative Commons Attribution 4.0 International License.
Read Full License

Additional Declarations: No competing interests reported.

Abstract

Purpose

Given the limitations of conventional stone burden assessment based on maximum diameter or ellipsoid-derived volume estimates, we aimed to develop an artificial intelligence (AI)–based method for automated quantification of stone and hydronephrosis volumes from CT images.

Materials and Methods

A 2-step algorithm was developed. First, a U-Net incorporating residual blocks, dense blocks, a morphology-aware block, and attention gates (RDAM U-Net) segmented the kidneys; hyperparameters were optimized using Complex System Response (CSR) experimental design with 5-fold cross-validation. Second, within the segmented kidney, hydronephrosis was identified from low–Hounsfield unit (HU) regions, and renal stones from high-HU regions using morphological processing and 3-dimensional (3D) connected-component analysis. AI-derived stone volumes were compared with ellipsoid-based estimates using Pearson and Spearman correlation, Lin's concordance correlation coefficient (CCC), intraclass correlation coefficient (ICC), and Bland–Altman analysis.

Results

Eighty-two kidney CT cases were used for model development. RDAM U-Net achieved a mean intersection over union of 0.9432 and Dice coefficient of 0.9681, with fewer parameters and a 32.58% shorter parameter-update time than reference attention-based U-Nets. In 39 paired stone measurements, AI-derived and ellipsoid-estimated volumes showed a near-perfect correlation (Pearson $r = 0.977$; Spearman $\rho = 0.966$; $R^2 = 0.954$; all $p < 0.001$) and high agreement (Lin's CCC = 0.959; ICC = 0.960). AI volumes were systematically lower than ellipsoid estimates (mean difference, − 51.21 mm^3; $p = 0.001$), with the difference increasing with stone volume. HU-based composition analysis agreed with the clinical record in 12 of 13 classifiable stones (92.3%).

Conclusions

AI-based CT segmentation enabled automated volumetric quantification of both urinary stone burden and hydronephrosis, providing direct 3D assessment without reliance on geometric assumptions. Integrating stone volume, hydronephrosis volume, and stone composition into a single automated workflow may support more individualized surgical and metabolic management of urolithiasis. Further validation in larger external cohorts is warranted.

Introduction

Urolithiasis affects an estimated 10.85% of adults worldwide.[1] Stone burden is a key determinant of management, and current guidelines stratify stones by cumulative linear diameter. Although stone volume better predicts stone-free status after surgery, its routine use is limited by measurement difficulty, lack of standardized reporting, and absence of validated volume thresholds.[2]

Urinary stones are complex, irregularly shaped 3D concretions, and a 1D or 2D assessment does not represent the true stone burden. Ellipsoid formulas rely on idealized shapes[3,4] and agree poorly with reference volumes determined by water displacement,[5] whereas 3D volumetric measurement is more reproducible than manual linear measurement.[6] Noncontrast CT (NCCT) is widely used for preoperative stone assessment and provides high spatial resolution and Hounsfield unit (HU) information for evaluating both stones and hydronephrosis.[7–9] However, manual measurement is operator-dependent and time-consuming.[10–12] Automated segmentation delineates the complete stone contour across consecutive slices and may provide a more accurate and reproducible assessment of true 3D stone burden.[13,14]

U-Net is among the most representative deep learning architectures for medical image segmentation, and attention gates (AGs) further suppress irrelevant background features.[15,16] Our group previously developed U-Net–based networks for hepatic and bladder tumor segmentation.[15–17] However, abdominal CT contains complex surrounding tissues, and model performance depends strongly on interacting hyperparameters such as batch size, epoch, and learning rate.[18–22]

Hydronephrosis, frequently caused by stone obstruction, may lead to renal dysfunction, infection, and irreversible renal damage if not treated promptly.[7–10,23,24] Hydronephrosis reflects pressure–volume changes within the upper urinary tract, and its quantitative volume has been associated with renal functional status beyond conventional grading.[25,26]

Given the shortcomings of current stone burden characterization, we aimed to develop and evaluate an AI algorithm for automated volumetric quantification of urinary stones and hydronephrosis from CT images, combining a Res-Dense-Attention-MAB U-Net (RDAM U-Net) for kidney segmentation with HU-based lesion analysis, and to compare AI-derived stone volume with the ellipsoid formula.

Materials and Methods

Algorithm Design

A 2-step algorithm was designed for fully automated kidney segmentation and lesion quantification (Fig. 1). In the first step, RDAM U-Net segments the kidneys. In the second step, the predicted kidney mask is used as the region of interest (ROI), within which HU-based image processing identifies hydronephrosis and renal stones. This study was approved by the Institutional Review Board of

Kaohsiung Medical University Hospital (KMUHIRB-E(I)-20250350) and informed consent was waived due to the retrospective nature of the study.

Step 1: kidney segmentation. RDAM U-Net retains the encoder–decoder architecture and skip connections of U-Net (Fig. 2). Residual blocks in the shallow encoder stages preserve low-level features and stabilize training; dense blocks in the deeper stages enhance feature reuse; a morphology-aware block (MAB) at the bottleneck aggregates multi-scale morphological features to strengthen kidney shape and boundary representation; and AGs in the decoder suppress background responses before feature fusion. A 1 × 1 convolution with sigmoid activation generates the binary kidney mask (Supplementary Figs. S1–S4). Five-fold cross-validation was used, and batch size (2–10), epoch (100–180), and learning rate (10^{-5}–10^{-3}) were optimized using CSR experimental design, which generated 13 representative combinations.

Step 2: lesion quantification. For hydronephrosis, the left and right kidneys were separated by 3D connected-component analysis, and a distance transform defined the renal core. Low-HU regions were selected as fluid candidates and refined using erosion, dilation, binary closing, hole filling, connected-component filtering, and adjacent-slice consistency checks. Hydronephrosis volume was calculated from voxel count and voxel spacing, and its ratio to ipsilateral kidney volume was reported. Renal stones were detected as high-HU voxels within the kidney ROI; binary closing and minimum connected-area filtering removed isolated noise, and candidate regions were labeled by 3D connected-component analysis so that a stone spanning multiple slices was treated as 1 lesion. For each stone, volume, side, upper/middle/lower renal location, and HU statistics were extracted. To reduce partial-volume effects, large stones were eroded in 3D before HU analysis, whereas small stones retained the original mask.

Data and Annotation

Abdominal CT data were provided by the collaborating hospital in DICOM format from patients with urolithiasis (n = 82). MITK Workbench was used to convert DICOM images to NIfTI format, preserving voxel spacing, slice thickness, and spatial orientation. Kidney ground-truth (GT) masks were manually delineated by clinical specialists. CT intensities were restored to HU using the NIfTI slope and intercept and normalized; images were resized from 512 × 512 to 224 × 224 pixels, and 5 augmentation strategies were applied (random crop and resize, scaling, affine transformation, horizontal flipping, and elastic transformation).

Reference Stone Volume Determination

Stone volume was estimated manually using the ellipsoid formula $V = 0.52 \times a \times b \times c$, where a, b, and c are the 3 orthogonal stone diameters measured on CT images (equivalent to $\pi \times a \times b \times c \times 0.167$, the scalene ellipsoid formula recommended by the European Association of Urology[27]). Volumes were expressed in mm^3, and only stones with paired AI-derived and manual measurements were analyzed.

Statistical Analysis

Kidney segmentation was evaluated against GT masks using IoU as the primary metric, with Dice coefficient, precision, recall, F1-score, and accuracy as secondary metrics.[28] Continuous variables were summarized as mean ± SD and median (IQR). The association between AI-derived and ellipsoid volumes was evaluated using Pearson's correlation; Spearman's rank correlation was added because volumes were right-skewed. Simple linear regression (AI volume as dependent variable) yielded the intercept, slope, and R^2. Agreement was assessed using Lin's CCC and absolute-agreement ICC(A,1). Bland–Altman statistics evaluated bias, with the difference defined as AI minus manual volume and 95% limits of agreement as the mean difference ± 1.96 SD; a 1-sample *t* test assessed whether the mean difference differed from zero, and proportional bias was assessed by regressing differences on means. 95% CIs for Spearman's ρ, Lin's CCC, and ICC were estimated from 20,000 bootstrap resamples. In the patient-level analysis, volume error was expressed as the absolute percentage difference between predicted and reference volumes. All tests were 2-sided with $p < 0.05$ considered significant. Analyses were performed using Python 3.12.14 (Python Software Foundation, Wilmington, Delaware).

Results

Kidney Segmentation

Eighty-two kidney CT cases with approximately 18–22 axial slices each (1,806 images) were used for model development, and augmentation yielded 5,418 training images. RDAM U-Net achieved the highest mean IoU (0.9432) and Dice coefficient (0.9681), exceeding Attention U-Net, Dense Attention U-Net, and Res Attention U-Net in IoU by 0.92%, 0.82%, and 0.99%, respectively, whereas precision, recall, F1-score, and accuracy were comparable (Table 1). RDAM U-Net contained 4,693,668 parameters and required 251 s for parameter updating, approximately 32.58% less than the average of the reference models. The CSR-predicted optimum (batch size 7, epoch 179, learning rate 1×10^{-3}) yielded an IoU of 0.9432, within 0.15% of the predicted value; learning rate was the only significant factor. Predicted kidney masks agreed well with GT, preserving bilateral kidney morphology and boundaries (Fig. 3).

Table 1
Segmentation performance and computational cost of U-Net–based models

Model	Parameters	Update time (s)	Mean IoU	Mean Dice	Precision	Recall	F1-score
RDAM U-Net	4,693,668	251	0.9432	0.9681	0.9751	0.9740	0.9738
Attention U-Net	35,238,293	428	0.9346	0.9639	0.9750	0.9719	0.9732
Dense Attention U-Net	14,363,845	400	0.9355	0.9672	0.9737	0.9738	0.9735
Res Attention U-Net	11,456,201	289	0.9340	0.9674	0.9744	0.9741	0.9738

Stone Volume: AI vs Ellipsoid Formula

Thirty-nine paired stone-volume measurements were analyzed. Mean AI-derived volume was 267.81 ± 336.31 mm³ (median, 106.29; IQR, 56.68–365.61), and mean ellipsoid volume was 319.01 ± 382.68 mm³ (median, 138.93; IQR, 70.86–416.73; Table 2). AI-derived volume correlated strongly with ellipsoid volume (Pearson's $r = 0.977$; 95% CI, 0.956–0.988; Spearman $\rho = 0.966$; 95% CI, 0.911–0.985; both $p < 0.001$; Fig. 4), and the regression explained 95.4% of the variability ($R^2 = 0.954$). The slope of 0.858 (95% CI, 0.798–0.919) indicated lower AI volumes, particularly for larger stones. Agreement was high (Lin's CCC, 0.959; 95% CI, 0.903–0.983; ICC, 0.960; 95% CI, 0.905–0.983). The mean difference was − 51.21 mm³ (95% CI, − 79.51 to − 22.90; $p = 0.001$), with 95% limits of agreement of − 227.98 to 125.57 mm³ and significant proportional bias (slope, − 0.130; $p < 0.001$).

Table 2
Comparison of AI-derived and ellipsoid-estimated stone volumes

Measure	Estimate	95% CI or additional result
No. paired measurements	39	—
AI-derived volume, mean ± SD, mm³	267.81 ± 336.31	—
AI-derived volume, median (IQR), mm³	106.29 (56.68–365.61)	—
Ellipsoid volume, mean ± SD, mm³	319.01 ± 382.68	—
Ellipsoid volume, median (IQR), mm³	138.93 (70.86–416.73)	—
Pearson correlation coefficient, r	0.977	0.956–0.988; p < 0.001
Spearman rank correlation coefficient, ρ	0.966	0.911–0.985; p < 0.001
Linear regression slope	0.858	0.798–0.919
Linear regression intercept	−6.03	—
Coefficient of determination, R^2	0.954	p < 0.001
Lin's concordance correlation coefficient	0.959	0.903–0.983
ICC(A,1), absolute agreement	0.960	0.905–0.983
Mean difference, AI minus ellipsoid, mm³	−51.21	−79.51 to − 22.90; p = 0.001
95% limits of agreement, mm³	−227.98 to 125.57	—
Proportional-bias slope	−0.130	p < 0.001

Abbreviations: AI, artificial intelligence; CI, confidence interval; ICC, intraclass correlation coefficient; IQR, interquartile range; SD, standard deviation.

Note: Confidence intervals for Spearman correlation, Lin CCC, and ICC were calculated using 20,000 bootstrap resamples. The measurement difference was defined as AI-derived volume minus manually calculated volume.

Hydronephrosis Quantification

The algorithm automatically delineated hydronephrosis and generated 3D volumetric reconstructions (Fig. 5). Because no clinical hydronephrosis GT label was available, these values are reported as model-derived fluid/hydronephrosis candidate volumes rather than diagnostic sensitivity or specificity.

Discussion

Stone burden predicts surgical complexity and treatment outcomes, yet manual volumetric measurement of irregular 3D stones is difficult and time-consuming, so maximum diameter remains the

common surrogate. [29,30] Linear measurement, however, is poorly reproducible: interobserver variability of 26.2% has been reported among radiologists,[6] corresponding to errors of 1.2 to 1.9 mm,[31] which makes it difficult to determine whether a 1- to 2-mm change during follow-up reflects true stone growth. The European Association of Urology guideline panel acknowledged that stone volume predicts stone-free status more accurately than linear size, yet its algorithms still stratify stones by cumulative diameter because accurate, rapid, and reproducible volumetry is not routinely available.[2,32] Automated AI-based segmentation may close the measurement and standardization components of this gap.[33]

Most prior AI models for urolithiasis on NCCT targeted stone detection rather than 3D quantification; only 42% of AI studies in a recent systematic review automated stone measurement.[34] Babajide et al. identified stones efficiently but with limited volumetric precision (Dice, 0.66).[35] Elton et al. reported a strong relationship between automated and manual volumes (R^2 = 0.95),[36] Mukherjee et al. tracked stone burden longitudinally with concordance correlation coefficients of 0.915 to 0.995,[37] and Cumpanas et al. reported R = 0.98 and Dice = 0.90 against 3D Slicer–based volumes, outperforming ellipsoid formulas.[33] Our algorithm extends these stone-only approaches by quantifying stone volume, hydronephrosis volume, and HU-based stone composition within a single automated workflow.

AI-derived volume correlated strongly with ellipsoid estimates, indicating that the algorithm reliably reflects relative differences in stone burden. Discrepancies were greater for larger stones; because the ellipsoid formula assumes a regular geometry, these likely reflect limitations of formula-based estimation rather than AI error. The direction of the discrepancy supports this interpretation. Cumpanas et al. found that ellipsoid formulas overestimated 3D Slicer–based volume by 27% to 89%, depending on stone size and shape,[33] and Finch et al. showed that no single ellipsoid formula fits all stone shapes.[27] In our cohort, mean ellipsoid volume exceeded mean AI volume by approximately 19%, and the difference increased with stone volume, consistent with ellipsoid overestimation rather than AI underestimation.

Technically, RDAM U-Net achieved the best overlap-based kidney segmentation among the compared architectures with fewer parameters and shorter parameter-update time. Its parameter count was approximately one-seventh that of Attention U-Net, which may facilitate deployment on standard clinical workstations, and CSR reproduced the predicted optimum within 0.15% using 13 runs instead of an exhaustive grid search.

Hydronephrosis reflects the upstream response of the urinary tract to obstruction, and its extensive, irregular geometry cannot be represented by a linear measurement or geometric formula. Quantitative hydronephrosis area predicted impacted ureteral stones better than the Society for Fetal Urology grade (AUC, 0.781 vs 0.676),[38] and preoperative hydronephrosis is a risk factor for ureteral stricture after endoscopic stone treatment.[39] Obstruction with poor pelvic compliance is associated with impaired renal function,[40] and CT-derived collecting-system geometry has been used to estimate renal pelvic pressure noninvasively.[41] AI-derived hydronephrosis volume could therefore be integrated with

collecting-system geometry and renal function to characterize individualized pressure–volume relationships and identify kidneys at risk of functional deterioration.

Volumetric assessment has direct clinical implications. Two stones with the same 10-mm maximum diameter may differ approximately 5-fold in volume,[33] which linear-based treatment algorithms cannot distinguish. Automated volumetry may also allow true stone growth to be separated from measurement error during metabolic follow-up, and preoperative identification of uric acid stones by HU-based composition analysis may select patients for oral dissolution therapy. Prospective studies are needed to determine whether volume-based thresholds improve treatment selection and stone-free outcomes.

This study has limitations. First, the dataset was small and from a single institution. Second, AI-derived volume was compared with ellipsoid-estimated rather than segmentation-based or physical reference volume; consequently, voxel-level stone Dice and Hausdorff distance could not be calculated, and the true gold standard—volume by water displacement or gas pycnometry—is rarely obtainable in the era of minimally invasive surgery. Third, the effects of CT acquisition parameters on segmentation were not evaluated. Fourth, images were resized to 224 × 224 pixels, which may reduce accuracy for small stones, and laterality labeling was inconsistent in several cases. Fifth, associations of AI-derived volume with treatment selection, operative time, stone-free status, and complications were not examined. Finally, hydronephrosis volume remains an exploratory imaging biomarker without a clinical GT label; prospective multicenter studies integrating volumetry with renal function, pressure-related parameters, and clinical outcomes are warranted.

Conclusions

AI-based CT segmentation enabled automated volumetric quantification of both urinary stone burden and hydronephrosis, with strong correlation and agreement with ellipsoid-based estimates and without reliance on geometric assumptions. Combining RDAM U-Net with HU-based lesion analysis provides an integrated, computationally efficient framework for clinical decision support. Further validation in larger external cohorts is warranted.

Declarations

Acknowledgements

This study was partially supported by NSYSU-KMU-115-P13, the Ministry of Science and Technology (NSTC 113-2324-B-037-027), Kaohsiung Medical University Hospital (KMUH-113-3R49, KMUH114-4M52), and Regenerative Medicine and Cell Therapy Research Center (KMU-TC114A202).

Author Contribution

AI radiomics analysis, AI model development: Ming-Chan Lee
Data analysis, Study conceptualization: Hsiang Ying Lee, Wei-Ming Li
Data collection: Chun-Kai Chang, Karl Marvin Tan, Jomari Jalipa
Manuscript drafting: Hsiang Ying Lee
Study supervision: Yow-Ling Shiue, Cheng-Tang Pan, Wen-Jeng Wu
Critical manuscript revision: Vineet Gauhar

References

1. Vera-Ponce VJ, Sanchez-Tamay NM, Ballena-Caicedo J, Zuzunaga-Montoya FE, De Gutierrez CI, Poemape Mestanza RL (2025) Global prevalence of urolithiasis: a meta-analysis accounting for methodological heterogeneity. Front Urol 5:1705953
2. Geraghty R, Pietropaolo A, Tzelves L, Lombardo R, Jung H, Neisius A et al (2024) Which measure of stone burden is the best predictor of interventional outcomes in urolithiasis: a systematic review and meta-analysis by the YAU Urolithiasis Working Group and EAU Urolithiasis Guidelines Panel. Eur Urol Open Sci 71:22–30
3. Panthier F, Doizi S, Illoul L, Berthe L, Traxer O (2021) Developing free three-dimensional software for surgical planning for kidney stones: volume is better than diameter. Eur Urol Focus 7:589–590
4. Peyrottes A, Chicaud M, Fourniol C, Doizi S, Timsit MO, Méjean A et al (2023) Clinical reproducibility of the stone volume measurement: a Kidney Stone Calculator study. J Clin Med 12(19):6274
5. Jain R, Omar M, Chaparala H et al (2018) How accurate are we in estimating true stone volume? A comparison of water displacement, ellipsoid formula, and a CT-based software tool. J Endourol 32(6):572–576
6. Patel SR, Stanton P, Zelinski N et al (2011) Automated renal stone volume measurement by noncontrast computerized tomography is more reproducible than manual linear size measurement. J Urol 186(6):2275–2279
7. Nuraj P, Hyseni N (2017) The diagnosis of obstructive hydronephrosis with color Doppler ultrasound. Acta Inf Med 25(3):178
8. Akram H, John A, Ali A, Jamil M, Rasheed L (2022) Role of CT-KUB for detection of obstructive and non-obstructive hydronephrosis on the basis of frequency of calculi. Pak BioMed J. :32–35
9. Bo S, Sedaghat F, Pavuluri K, Rowe SP, Cohen A, Kates M, McMahon MT (2021) Dynamic contrast enhanced-MR CEST urography: an emerging tool in the diagnosis and management of upper urinary tract obstruction. Tomography 7(1):80–94
10. Yuruk E, Tuken M, Sulejman S, Colakerol A, Serefoglu EC, Sarica K, Muslumanoglu AY (2017) Computerized tomography attenuation values can be used to differentiate hydronephrosis from pyonephrosis. World J Urol 35(3):437–442
11. Nie S, Jia N, Chen H, Chen R, Geng J, Shao X et al (2025) Artificial intelligence-assisted diagnosis of glomerular nephritis using a pathological image analysis approach: a multicentre model development and validation study. EClinicalMedicine. ;89

12. Vijayakumar M, Ganpule A, Singh A, Sabnis R, Desai M (2018) Review of techniques for ultrasonic determination of kidney stone size. Res Rep Urol. :57–61
13. Panthier F, Kutchukian S, Ducousso H, Doizi S, Solano C, Candela L et al (2024) How to estimate stone volume and its use in stone surgery: a comprehensive review. Actas Urol Esp (Engl Ed) 48(1):71–78
14. Jain R, Maskal S, Milk J et al (2021) Utility of stone volume estimated by software algorithm in predicting success of medical expulsive therapy. Can Urol Assoc J 15:E144–E147
15. Chen WF, Ou HY, Lin HY, Wei CP, Liao CC, Cheng YF, Pan CT (2022) Development of novel residual-dense-attention (RDA) U-Net network architecture for hepatocellular carcinoma segmentation. Diagnostics 12(8):1916
16. Lee MC, Wang SY, Pan CT, Chien MY, Li WM, Xu JH, Luo CH, Shiue YL (2023) Development of deep learning with RDA U-Net network for bladder cancer segmentation. Cancers 15(4):1343
17. Chen WF, Ou HY, Liu KH, Li ZY, Liao CC, Wang SY, Huang W, Cheng YF, Pan CT (2021) In-series U-Net network to 3D tumor image reconstruction for liver hepatocellular carcinoma recognition. Diagnostics 11(1):11
18. Wong TT, Yeh PY (2020) Reliable accuracy estimates from k-fold cross validation. IEEE Trans Knowl Data Eng 32(8):1586–1594
19. Yates LA, Aandahl Z, Richards SA, Brook BW (2023) Cross validation for model selection: a review with examples from ecology. Ecol Monogr 93(1):e1557
20. Kandel I, Castelli M (2020) The effect of batch size on the generalizability of the convolutional neural networks on a histopathology dataset. ICT Express 6(4):312–315
21. Zhang C, Bengio S, Hardt M, Recht B, Vinyals O (2021) Understanding deep learning (still) requires rethinking generalization. Commun ACM 64(3):107–115
22. Wu Y, Liu L, Bae J, Chow KH, Iyengar A, Pu C, Wei W, Yu L, Zhang Q (2019) Demystifying learning rate policies for high accuracy training of deep neural networks. In: Proc 2019 IEEE Int Conf Big Data. :1971–1980
23. Esmaeili M, Esmaeili M, Ghane F, Alamdaran A (2016) Comparison between diuretic urography (IVP) and diuretic renography for diagnosis of ureteropelvic junction obstruction in children. Iran J Pediatr 26(1):e4293
24. Aseme S, Tsegaye AM, Tilahun SB, Mammo TN (2024) A case report of congenital ureteral stricture: obstructed, hydronephrotic solitary kidney with cystic dysplastic changes. Int J Surg Case Rep 120:109818
25. Saha T, Trivedi S, Dwivedi AN (2025) Correlation of radiological volume parameters using magnetic resonance imaging with surgical intervention, postoperative outcome, and renal function in adult patients of pelvic ureteric junction obstruction. Acta Radiol 66(11):1149–1158
26. Zheng MM, Zhu YC, Shang LM, Du CK, Zhang L, Sun W et al (2022) Use of CT-based renal volumetry for the measurement of split renal function: a split glomerular filtration rate prediction model based on unilateral renal volume parameters. Clin Radiol 77(10):759–766

27. Finch W, Johnston R, Shaida N, Winterbottom A, Wiseman O (2014) Measuring stone volume—three-dimensional software reconstruction or an ellipsoid algebra formula? BJU Int 113(4):610–614
28. Taha AA, Hanbury A (2015) Metrics for evaluating 3D medical image segmentation: analysis, selection, and tool. BMC Med Imaging 15:29
29. Okhunov Z, Friedlander JI, George AK, Duty BD, Moreira DM, Srinivasan AK et al (2013) S.T.O.N.E. nephrolithometry: novel surgical classification system for kidney calculi. Urology 81(6):1154–1159
30. Panthier F, Alvarez E, Gauhar V, Crawford-Smith H, Allen S, Bin Hamri S et al (2025) Stone volume instead of maximum stone diameter: results from an international survey. BJU Int 136(1):95–102
31. Eisner BH, Kambadakone A, Monga M et al (2009) Computerized tomography magnified bone windows are superior to standard soft tissue windows for accurate measurement of stone size: an in vitro and clinical study. J Urol 181(4):1710–1715
32. European Association of Urology (2026) EAU Guidelines on Urolithiasis. Edition presented at the EAU Annual Congress London 2026. EAU Guidelines Office, Arnhem, the Netherlands
33. Cumpanas AD, Chantaduly C, Morgan KL, Shao W, Gorgen ARH, Tran CM et al (2024) Efficient and accurate computed tomography-based stone volume determination: development of an automated artificial intelligence algorithm. J Urol 211(2):256–265
34. Panthier F, Melchionna A, Crawford-Smith H et al (2024) Can artificial intelligence accurately detect urinary stones? A systematic review. J Endourol 38(8):725–740
35. Babajide R, Lembrikova K, Ziemba J et al (2022) Automated machine learning segmentation and measurement of urinary stones on CT scan. Urology 169:41–46
36. Elton DC, Turkbey EB, Pickhardt PJ, Summers RM (2022) A deep learning system for automated kidney stone detection and volumetric segmentation on noncontrast CT scans. Med Phys 49(4):2545–2554
37. Mukherjee P, Lee S, Elton DC, Nakada SY, Pickhardt PJ, Summers RM (2023) Fully automated longitudinal assessment of renal stone burden on serial CT imaging using deep learning. J Endourol 37(8):948–955
38. Iwahashi Y, Kohjimoto Y, Deguchi R, Wakamiya T, Yamashita S, Hara I (2024) Area of hydronephrosis is a useful predictive factor of impacted ureteral stones. Urolithiasis 52(1):56
39. Moretto S, Saita A, Scoffone CM et al (2024) Ureteral stricture rate after endoscopic treatments for urolithiasis and related risk factors: systematic review and meta-analysis. World J Urol 42(1):234
40. Bullock KN, Whitaker RH (1984) Upper urinary tract compliance: its importance in obstructive hydronephrosis. Ann Acad Med Singap 13(4):585–589
41. Nishimura K, Imada S, Sugihara N et al (2025) Novel modality using computational fluid dynamics to estimate renal pelvic pressure and evaluate severity of obstruction in congenital hydronephrosis. Front Urol 5:1634278

Figures

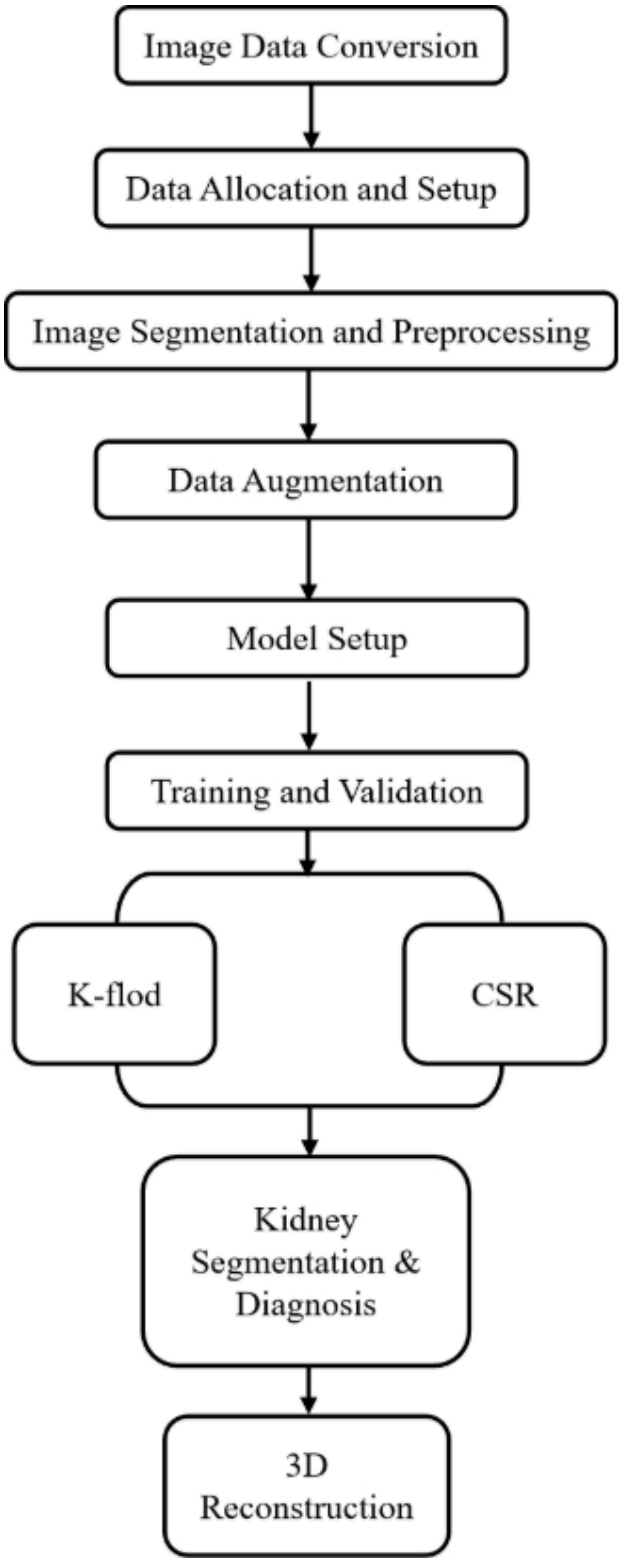


Figure 1

Algorithm design and overall experimental workflow.

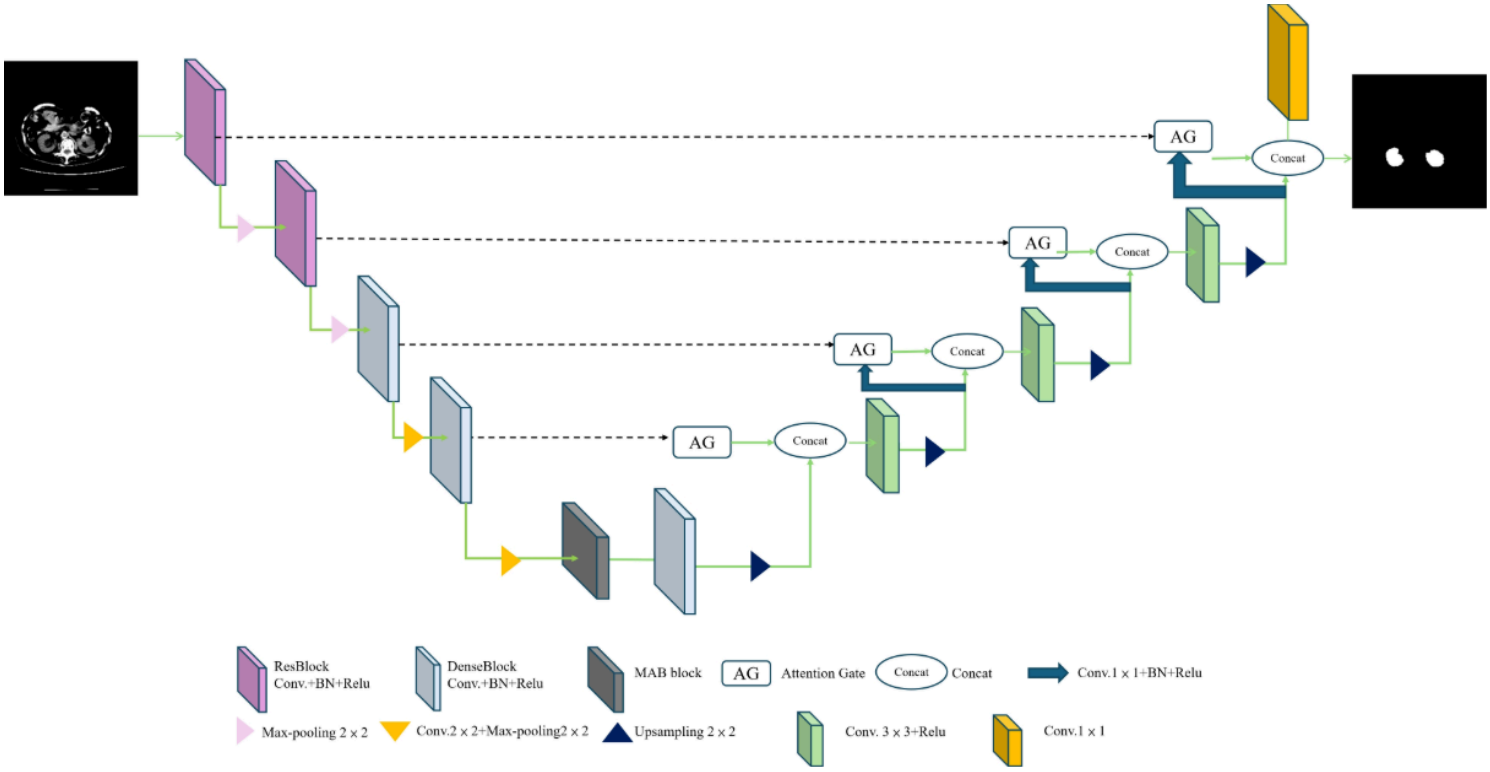


Figure 2

Architecture of the proposed RDAM U-Net.

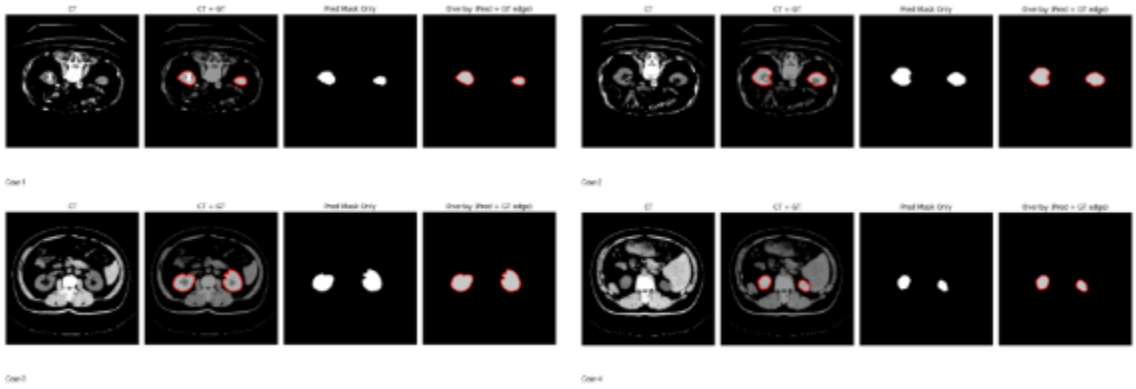


Figure 3

Representative kidney segmentation results: CT, CT + GT, predicted mask, and prediction/GT overlay.

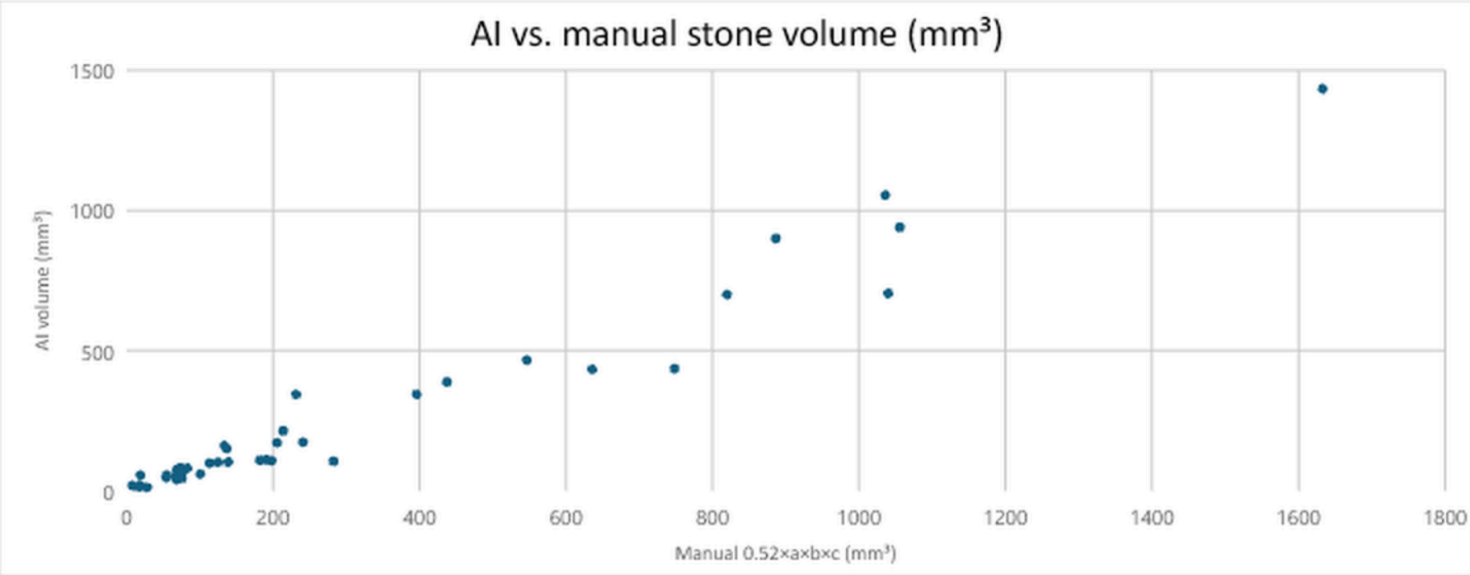


Figure 4

Association between AI-derived and manually calculated stone volumes. The scatter plot shows the relationship between stone volume automatically calculated by the AI model and stone volume manually estimated using the 0.52 × a × b × c formula. Each point represents one paired stone measurement (Pearson r=0.977, 95% CI 0.956-0.988; p<0.001).

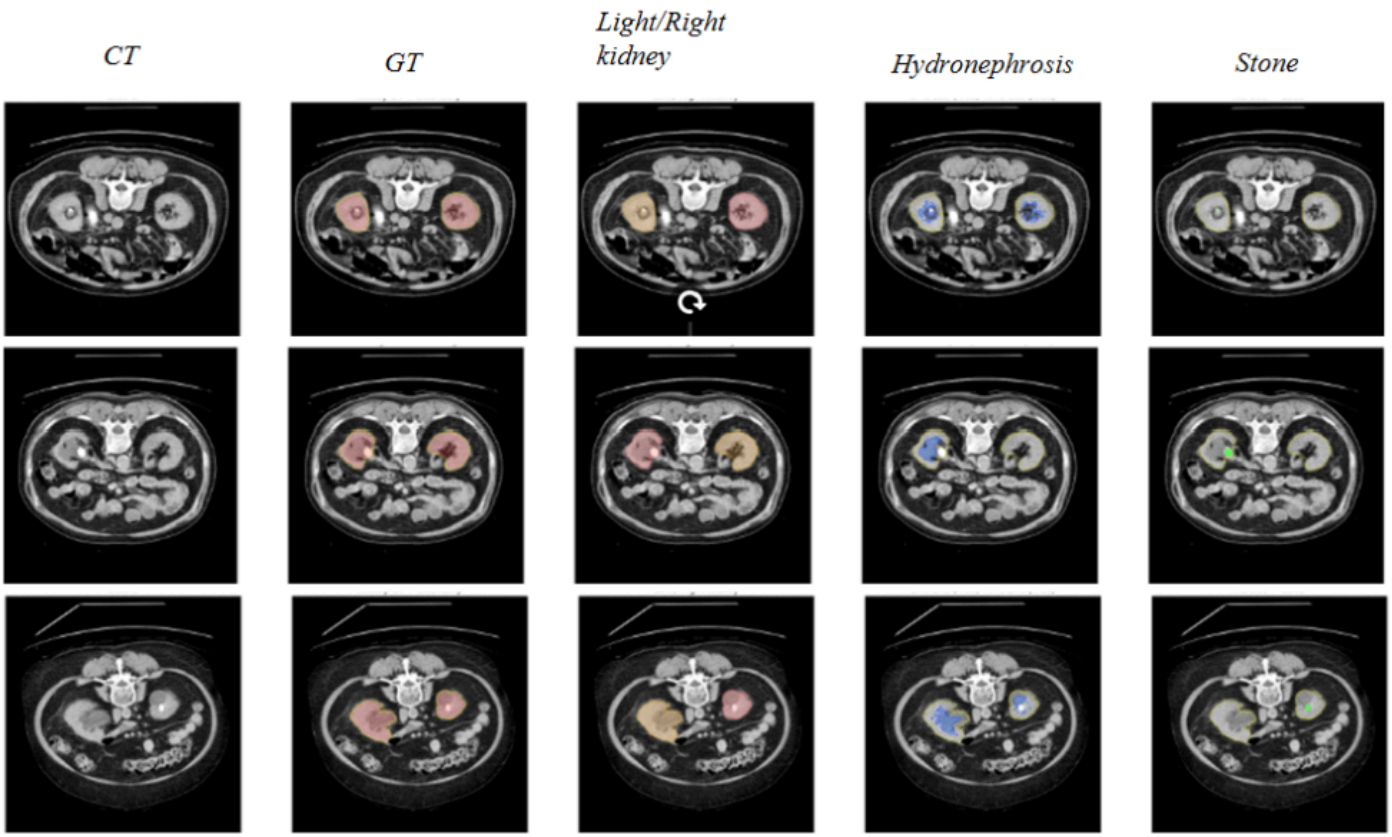


Figure 5

Representative lesion-analysis outputs. Orange/red indicates the 2 kidneys, blue indicates hydronephrosis candidate regions, and green indicates renal stone candidate regions.

Supplementary Files

This is a list of supplementary files associated with this preprint. Click to download.

- SupplementaryMaterial.docx